




Article

Study of Fire Plume Behavior and Maximum Ceiling Temperature Rise in a Curved Tunnel Driven by the Coupling of Blockage Effect and Longitudinal Ventilation

Xin Zhang ¹, Jie Li ¹, Hao He ¹, Xiaofeng Chen ^{2,3}, Kai Zhu ⁴, Mingjian Yin ⁴, Ying Cao ⁵ and Ke Wu ^{2,3,*}

¹ College of Electronic Engineering, Xi'an Shiyou University, Xi'an 710065, China; candyzhang@zju.edu.cn (X.Z.); 21212030432@stumail.xsyu.edu.cn (J.L.); 23212030502@stumail.xsyu.edu.cn (H.H.)

² Center for Balance Architecture, Zhejiang University, Hangzhou 310027, China; xiaofengchen@zju.edu.cn

³ Research Center for Urban Fire Safety Engineering, Zhejiang University, Hangzhou 310058, China

⁴ College of Energy Environment and Safety Engineering, China Jiliang University, Hangzhou 310018, China; zhukai@cjlju.edu.cn (K.Z.); yinmingjian@cjlju.edu.cn (M.Y.)

⁵ Zhejiang University Urban and Rural Planning and Design Research Institute Co., Ltd., Hangzhou 310058, China; 0921871@zju.edu.cn

* Correspondence: wuke@zju.edu.cn

Abstract: Tunnel fires often lead to vehicles being trapped inside, causing the “blocking effect”. In this work, fire plume behavior and the maximum ceiling temperature rise in a curved tunnel with blocked vehicles under longitudinal ventilation conditions are studied numerically. The results show that, in curved tunnels, the fire plume in the quasi-stable state exhibits dynamic deflections between the concave and convex walls of the tunnel, so the location of high-temperature zones varies accordingly. The flow field structure in the near field of the blockage and the fire source is complex but can be decoupled into four characteristic sub-structures, i.e., the free shear layer, recirculation I above the vehicle blockage, recirculation II behind the downstream of the blockage, and recirculation III at the top of the tunnel. Recirculation I and II pull the fire plume upstream, while free shear layer and recirculation III pull the flame downstream. The final plume deflection direction depends on the relative strengths of these two pulling forces. As the longitudinal air velocity increases, the plume deflection direction changes from downstream to upstream of the fire source, forming the “downstream tilt—touch the ceiling above the fire source—upstream tilt” mode, resulting in the maximum ceiling temperature rise fluctuating in a decreasing-increasing-decreasing trend. Moreover, the higher the blocking ratio, the lower the critical air velocity required to induce the transition of the plume deflection directions, e.g., a critical wind speed of 3 m/s for a blockage ratio of 0.46 and a critical wind speed of 1 m/s for a blockage ratio of 0.62. Finally, a semi-empirical equation of the maximum ceiling temperature rise in curved tunnels, considering both longitudinal wind and the vehicle blocking ratio, is proposed and validated. This work highlights the multi-dimensional and non-stable plume behavior pattern in a complex tunnel fire scenario, thus providing a deeper understanding to improve the classical tunnel fire dynamic system.

Keywords: maximum temperature rise; blocking rate; fire plume behavior; curved tunnel



Academic Editor: Zihao Gao

Received: 19 November 2024

Revised: 17 December 2024

Accepted: 24 December 2024

Published: 27 December 2024

Citation: Zhang, X.; Li, J.; He, H.; Chen, X.; Zhu, K.; Yin, M.; Cao, Y.; Wu, K. Study of Fire Plume Behavior and Maximum Ceiling Temperature Rise in a Curved Tunnel Driven by the Coupling of Blockage Effect and Longitudinal Ventilation. *Fire* **2025**, *8*, 9. <https://doi.org/10.3390/fire8010009>

Copyright: © 2024 by the authors.

Licensee MDPI, Basel, Switzerland.

This article is an open access article distributed under the terms and conditions of the Creative Commons

Attribution (CC BY) license

(<https://creativecommons.org/licenses/by/4.0/>).

1. Introduction

Highway tunnels are vital for easing urban congestion and reducing travel distances [1–3]. Fire poses a significant safety risk in tunnels due to their semi-closed design, allowing high

temperatures and toxic smoke to accumulate and potentially cause casualties [4–6]. Structural integrity is also at risk from exposure to flames and hot smoke, with the potential for damage or collapse if the smoke's high-temperature load exceeds the tunnel ceiling's bearing capacity [7–12]. Such incidents lead to extensive maintenance, traffic disruptions, and economic losses. Notable examples include the Mont Blanc Tunnel fire, which caused severe damage to the tunnel ceiling and a three-year traffic disruption, and the 2019 Maoliling Tunnel fire in Zhejiang Province, resulting in significant structural damage, a week-long traffic disruption, and a direct economic loss of 5 million RMB. Therefore, ensuring proper fire protection to limit the maximum temperature at the tunnel ceiling during a fire is a critical focus of tunnel fire research.

During the 1950s and 1980s, scholars extensively researched fire plume modeling, proposing an ideal plume mass flow rate model using axisymmetric and high-cap models [13–15], conducted theoretical analysis and developed a prediction model for ceiling temperature rise under natural ventilation conditions, applying the ceiling jet theory and energy conservation principles. Notably, this model is specific to scenarios where the fire plume impacts an infinite roof ceiling without wind, excluding confined spaces like tunnels. Kurioka et al. [16] conducted scale modeling and full-scale experiments, introducing a ceiling maximum temperature rise prediction model for straight tunnels, as shown in Equation (1). This model considers the dimensionless heat release rate, Froude number, and the impact of longitudinal air velocities within tunnels.

$$\begin{aligned} \frac{\Delta T_{max}}{T_0} &= \gamma \left(\frac{Q^{*2/3}}{Fr^{1/3}} \right)^\varepsilon \\ \frac{Q^{*2/3}}{Fr^{1/3}} &< 1.35, \gamma = 1.77, \varepsilon = 6/5 \\ \frac{Q^{*2/3}}{Fr^{1/3}} &\geq 1.35, \gamma = 2.54, \varepsilon = 0 \end{aligned} \quad (1)$$

where ΔT_{max} is the maximum temperature rise in the tunnel ceiling in K, Fr is the Froude number, and Q^* is the dimensionless heat release rate of the fire source, with their expressions given as follows:

$$Fr = \frac{u^2}{gH_{ef}} \quad (2)$$

$$Q^* = \frac{Q}{\rho_0 c_p T_0 g^{1/2} H_{ef}^{5/2}} \quad (3)$$

where u is the longitudinal velocity of the tunnel in m/s, g is the acceleration of gravity in m/s^2 , H_{ef} is the effective tunnel height (the vertical distance from the fire source surface to the tunnel ceiling) in m, Q is the heat release rate of the fire source in kW, ρ_0 is the density of the air in kg/m^3 , c_p is the constant-pressure heat capacity of the air in $kJ/kg \cdot K$, and T_0 is the atmosphere temperature in K.

However, Li et al. [17] discovered that Kurioka's model [16] shows significant inaccuracies in predicting the maximum temperature increase at the tunnel ceiling during fires with low longitudinal air velocities. They introduced a dimensionless parameter, u' , to assess the impact of longitudinal air velocity on this temperature rise. Their findings suggest that for $u' \leq 0.19$, the tunnel ceiling's maximum temperature rise is primarily influenced by the heat release rate, following a power law with an exponent of 2/3. Conversely, for $u' > 0.19$, the temperature rise decreases linearly with increasing longitudinal ventilation speed and increases linearly with the heat release rate. By using $u' = 0.19$ as the boundary, they developed a segmented predictive model for the maximum temperature rise in a straight tunnel ceiling, as shown in Equation (4).

$$\Delta T_{max} = \begin{cases} \frac{Q}{ur^{1/3}H_{ef}^{5/3}}, & u' > 0.19 \\ 17.5 \frac{Q^{2/3}}{H_{ef}^{5/3}}, & u' \leq 0.19 \end{cases} \quad (4)$$

$$u' = \frac{u}{w^*}, \quad w^* = \left(\frac{Q_c g}{r \rho_0 c_p T_0} \right)^{1/3} \quad (5)$$

where r is the radius of the fire source in m, w^* is the plume characteristic speed in m/s, and Q_c is the fire source convective heat release rate, typically 70% of the total heat release rate of the fire source, kW.

The study mentioned the fire source being at ground level, but in real fire scenarios, the fire source can have a specific height, which may cause tunnel blockages [18–21]. These blockages can significantly affect the fire plume characteristics at the tunnel ceiling, resulting in a change in the maximum temperature rise. To investigate this, Chen et al. [19] conducted a small-scale tunnel fire experiment and found that the maximum temperature rise of the ceiling gradually increased with the height of the fire source. Li et al. [20] introduced a fire source blockage rate factor and adjusted Kurioka's model to predict the ceiling's maximum temperature rise, while Zhong et al. [21] investigated the coupling effect of longitudinal air velocity and fire source height on the fire plume behavior and ceiling temperature rise in tunnels. They found that as the longitudinal air velocity increased, the fire plume gradually deflected downstream, leading to a significant reduction in the maximum temperature rise of the ceiling. Building on Li's model, a segmented prediction model was developed to forecast the tunnel ceiling's maximum temperature rise, accounting for longitudinal air velocity and fire source height variations.

Although the studies mentioned above were conducted in an ideal fire scenario with no vehicles near the fire source, in reality, tunnel fires often trap moving vehicles within the tunnel. The presence of vehicles upstream of the fire source can significantly alter the flow field structure inside the tunnel, causing the fire dynamics to differ from that of a tunnel without obstructive vehicles. Previous experiments have shown that blocked vehicles can cause the fire plume to draw in air asymmetrically from both sides, creating a complex and disordered flow field structure. This leads to an unstable temperature distribution of smoke in tunnel fires and an increased risk of fire [22]. Compared to the unobstructed situation, the maximum temperature rise of the tunnel ceiling increases by 300% [23]. Currently, many scholars focus on various aspects of building fire prevention, structural fire resistance, and smoke control when researching the key characteristic parameters that reflect the smoke transport characteristics in straight tunnels. They consider different blocking factors such as vehicle the blocking ratio, distance between the vehicle blocking object and the fire source, length of the vehicle blocking, distance between the vehicle blocking object and the tunnel sidewalls, and height of the vehicle blocking object from the tunnel floor. These parameters include the temperature distribution and maximum temperature rise of the ceiling jet [23–26], the length of the smoke backflow layer [27–29], and the critical velocity [30]. To facilitate prompt information about these characteristic parameters and effectively respond to emergencies, researchers have quantified the effects of various blocking factors. They have also developed and validated a series of universal prediction models for the maximum temperature of the smoke flow under the tunnel ceiling, longitudinal temperature decay under the tunnel ceiling, length of the smoke backflow layer, and critical velocity.

It should be noted that the above studies have been conducted on straight tunnels. However, road tunnels are often characterized by curved structures due to the type of inter-

section, site conditions, and other factors [31,32]. Examples include high-curvature ramps in bifurcated tunnels (such as the Nanterre-La Défense Tunnel in France), intersections of tunnel complexes connected with underground structures (like the Blanka Tunnel Complex in the Czech Republic), and spiral sections for overcoming the height difference between the two ends of the tunnel (e.g., Tiezhaizi 1# Tunnel and Ganhaizi Tunnel in China). In a curved tunnel with obstructed vehicles, a fire can initiate complex smoke movement influenced by ventilation speed, centrifugal force, buoyancy, and blockage effects. Therefore, the behavioral patterns and temperature distribution of the fire plume differ from those in straight tunnels. However, less attention has been paid to the motion characteristics of the curved tunnel fire plume and the maximum temperature rise of the tunnel vault under the blockage effect and the coupling of longitudinal ventilation.

In this paper, a three-dimensional mathematical model of a curved tunnel fire with blocked vehicles is constructed using the fire dynamics method and Fluent 2019R2. The model analyzes the flow field structure of the fire within the curved tunnel under the combined influence of longitudinal ventilation conditions and the effect of vehicle blocking. The study clarifies the transverse and longitudinal movement behavioral characteristics of the fire plume in the curved tunnel and establishes the variation law of the maximum temperature rise at the tunnel ceiling. Based on this, a semi-empirical equation of the maximum temperature rise at the curved tunnel ceiling that considers both longitudinal wind and the vehicle blockage ratio is proposed, which could well reflect the trend and guide engineering applications. The research findings can offer scientific theoretical guidance for the installation of fire-fighting equipment, such as smoke detectors and fire extinguishing nozzles, in longitudinally ventilated curved tunnels with blocked vehicles.

2. Mathematical Modeling

2.1. Control Equation

The development process of fire is a complex phenomenon that involves fluid dynamics, heat transfer, and combustion. It is governed by the laws of physics and chemistry, as well as fundamental control equations, including mass, momentum, energy, and component conservation equations, along with the ideal gas equation of state [33].

When a fire occurs in a tunnel, the high temperature from combustion reduces the gas density near the combustion point, causing turbulent air flow in the tunnel, regardless of whether it is ventilated or not. The k - ϵ model based on Reynolds averaging is widely used in engineering [34] due to its good balance between calculation accuracy and volume, except for swirling flow. The RNG k - ϵ model improves the k - ϵ equations by establishing a relation for the variation of model constant $C_{\epsilon 3}$ with the Richardson number. It can consider the effects of swirling flow and curved walls on the turbulent structure, making it suitable for simulating fire scenarios in curved tunnels [31]. Therefore, the RNG k - ϵ model with buoyancy correction is selected to account for the turbulence effect in this paper.

The combustion process of a real tunnel fire is complex and involves multiple components and primitive reactions, making it difficult to describe quantitatively with a single chemical reaction equation. However, for practical engineering purposes, the focus is on the average reaction rate, final thermal effect, and resulting changes in temperature, components, and flow field distribution. To simulate the fire source, this paper uses the PDF non-premixed combustion module in Fluent 2019R2, a fluid dynamics software, based on the mixing fraction model and fast response assumption. The P -1 model, which is more suitable and robust for combustion systems with complex geometries, is utilized for the radiation model [35]. The turbulent convection model, coupled wall, and Fourier's law-based heat conduction equation are adopted to solve the heat transfer in the fluid,

fluid–solid interface, and solid body, respectively. The SIMPLE algorithm is employed to solve the coupled velocity and pressure fields.

2.2. Model Description and Boundary Conditions

The simulated curved tunnel is 200 m long, with a cross-section size of 13.2 m (width) \times 6.6 m (height) and a radius of 400 m. The fire source, sized 2 m \times 2 m \times 2 m and having a steady-state heat release rate of 5 MW, similar to that of a car or minibus, is located on the centerline of the tunnel, 100 m from the entrance. To study the effect of blocking vehicles on smoke spread from a fire in the curved tunnel, the blocking vehicle was placed 5 m upstream of the fire source. A schematic diagram of the fire scenario in the curved tunnel with blocking vehicles is shown in Figure 1.

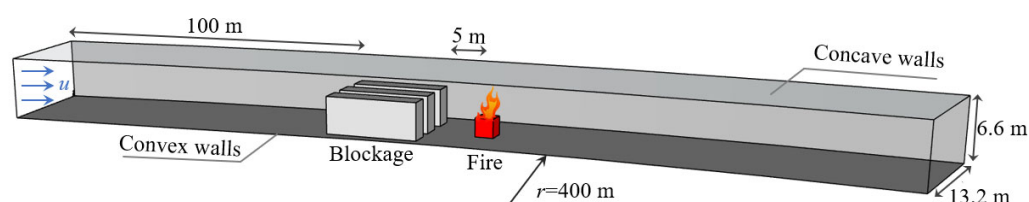


Figure 1. Schematic diagram of a fire scenario in a curved tunnel with blocked vehicles.

Considering the realistic vehicle size, and referring to the existing literature on vehicle blockage size settings [36], this paper simplifies the blockage vehicle size uniformly to 10 m (length) \times 2.2 m (width), and its cross-sectional area varies by adjusting the height from 0 to 5.4 m. Figure 2 illustrates the tunnel cross-section for different heights of the blocking vehicle. The blocking ratio φ is defined as the ratio of the vehicle's cross-sectional area to that of the tunnel, ranging from 0 to 0.62 in this paper. Additionally, the impact of longitudinal ventilation velocity, ranging from 1 to 4 m/s, on the flow of fire smoke and the temperature distribution in the fire scenario is also considered. The specific conditions studied in this paper are summarized in Table 1.

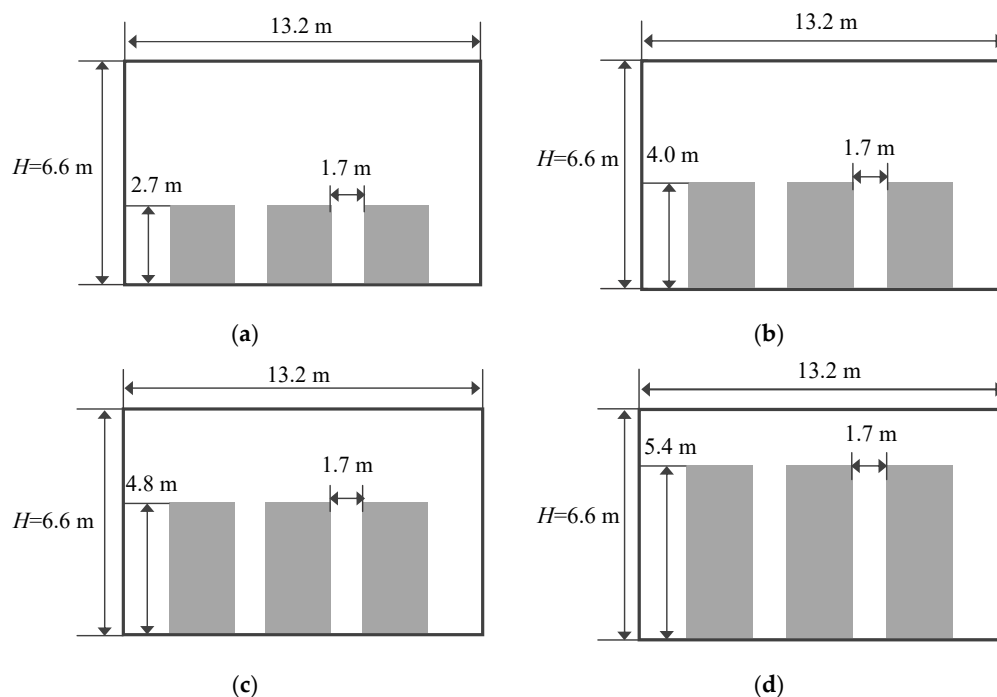


Figure 2. Blocked vehicle dimensions for each blocking ratio: (a) $\varphi = 0.31$; (b) $\varphi = 0.46$; (c) $\varphi = 0.55$; (d) $\varphi = 0.62$.

In the calculation, the tunnel inlet has a Dirichlet boundary condition with a given air velocity, while the tunnel outlet has a Neumann boundary condition with free outflow. The tunnel wall and road surface have a no-penetration-non-slip boundary with a surface roughness height of 0.025 m [6]. The wall’s thermal conductivity is 1.28 W/(m·K), referring to concrete with a density of 2500 kg/m³ and a thickness of 1 m. The specific heat capacity is 980 J/(kg·K). The top surface of the fire source is set as a mass flow rate boundary, with propane as the fuel. The mass flow rate is calculated by dividing the design heat release rate by the effective heat of combustion.

Table 1. Fire conditions.

NO.	Blocking Ratio φ	Longitudinal Ventilation Velocity u (m/s)
1–5	0	1.0, 2.0, 2.5, 3.0, 4.0
6–10	0.31	1.0, 2.0, 2.5, 3.0, 4.0
11–15	0.46	1.0, 2.0, 2.5, 3.0, 4.0
16–20	0.55	1.0, 2.0, 2.5, 3.0, 4.0
21–25	0.62	1.0, 2.0, 2.5, 3.0, 4.0

2.3. Grid and Time Step Sensitivity Analysis

Optimizing the grid size and time step is crucial for achieving accurate results and maximizing computational efficiency. Previous studies [37–41] suggest that the grid size should be within the range of 0.0625D* to 0.25D* (where D* represents the characteristic fire diameter, calculated as shown in Equation (6)).

$$D^* = \left(\frac{Q}{\rho_0 c_p T_0 \sqrt{g}} \right)^{2/5} \tag{6}$$

For a 5 MW fire, the reasonable grid size ranges from 0.125 m to 0.5 m, according to Equation (6). To validate grid sensitivity, four grid sizes (0.2 m, 0.25 m, 0.3 m, and 0.4 m) are selected. The computational domain is dissected using a hexahedral mesh. To ensure computational accuracy and efficiency, local refinement is implemented in the near field of the fire source (from 20 m upstream to 40 m downstream of the fire source). Additionally, the mesh size in the far field of the fire source is twice that of the near field [42], as shown in Figure 3. The four meshing schemes are presented in Table 2.

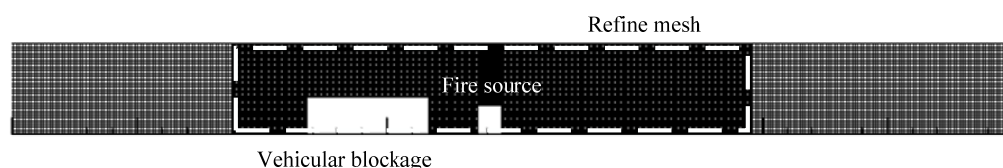


Figure 3. Schematic diagram of grid.

Table 2. Grid independence test cases.

Grid No.	Coarse Grid Cell Size (m)	Refine Grid Cell Size (m)	Total Grid Number
1	0.5	0.25	510,818
2	0.3	0.15	2,198,974
3	0.25	0.125	3,582,249
4	0.2	0.1	5,303,592

Figure 4 shows the longitudinal temperature distributions at 0.01 m below the ceiling in the downstream of the tunnel fire source within 0–10 m for a fire scenario with a curve radius of R = 400 m, heat release rate of Q = 5 MW, longitudinal air velocity of u = 1 m/s, and

blockage ratio of $\varphi = 0.31$, under the four grid schemes. It is observed that the temperature distributions under grid schemes 3 and 4 are the most similar. Using the mesh scheme of $0.2 + 0.1$ m (scheme 4) as the benchmark, the maximum relative errors of the temperatures for grid schemes 1, 2, and 3 are 4.06%, 2.90%, and 0.34%, respectively.

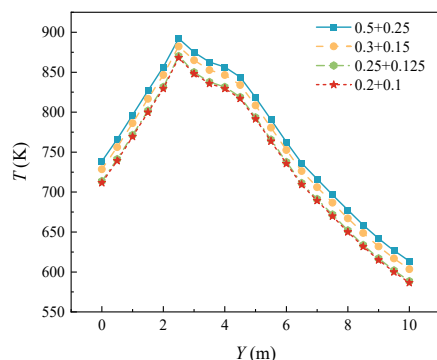


Figure 4. Longitudinal distribution of tunnel ceiling temperature under different grid cell sizes.

For the time step sensitivity study, time steps of 0.5 s, 2 s, 3 s, and 4 s are used. Figure 5 shows the longitudinal temperature distribution at 0.01 m below the tunnel ceiling for a fire scenario with a curve radius $R = 400$ m, fire source heat release rate $Q = 5$ MW, and longitudinal air velocity $u = 1.0$ m/s, calculated under the four time step scenarios. The longitudinal temperature distribution pattern is found to be similar in all four scenarios. Using the 0.5 s time step size scenario (Scenario 1) as a benchmark, the maximum errors of the temperature for the 2 s, 3 s, and 4 s time step scenarios are 0.04%, 10.48%, and 10.56%, respectively.

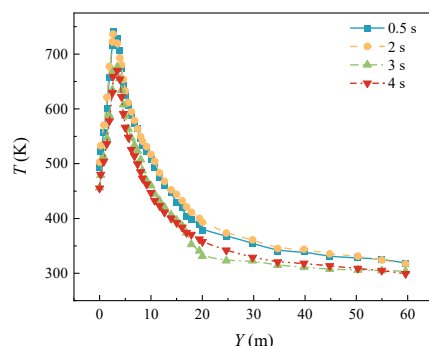


Figure 5. Longitudinal distribution of tunnel ceiling temperature under different time steps.

In summary, a grid of 0.125 m and a time step of 2 s are sufficient to capture the temperature changes of the current fire scenario. Therefore, this scheme is adopted as the basis for mesh splitting and time step setting for other working conditions in this paper.

The maximum temperature of the tunnel ceiling surface is chosen as the monitoring parameter for the calculation. The smoke flow is considered to reach a quasi-steady state when its fluctuation is less than 6% [6]. For the fire scenario with a curve radius $R = 400$ m, heat release rate of the fire source $Q = 5$ MW, longitudinal air velocity $u = 1.0$ m/s, and blocking ratio $\varphi = 0$, the variation of the maximum temperature with time at 30 m downstream of the fire source and 0.01 m under the ceiling is statistically presented in Figure 6. It is observed that the temperature fluctuation decreases after the fire has been burning for 300 s, with a fluctuation of less than 6.5%. Therefore, the maximum temperatures at the tunnel ceiling presented in the rest of this paper are all averaged over the time period from 360 s to 420 s.

The computational cases mentioned in the paper were carried out on a high-performance computing center, where the servers used for the calculations had dual 8573 processors, which could provide 64 physical cores (number of threads *3) for simultaneous computation, as well as 256 G of computing memory and 4 TB of storage space, with a base frequency of 2.3 GHz. Calculating a single case typically takes 7–10 h.

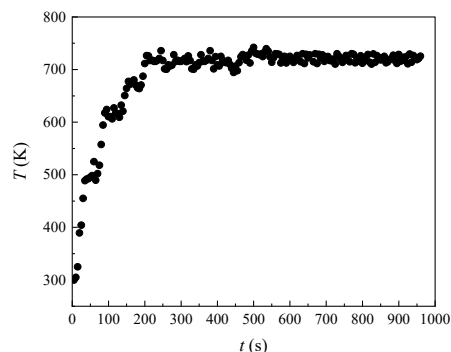


Figure 6. Variation of maximum temperature with time at 30 m downstream of the fire source and 0.01 m below the ceiling.

2.4. Validation of Numerical Models

The use of Fluent 2019R2 to simulate tunnel fire scenarios proves convenient and effective. Furthermore, it can compensate for the deficiencies of physical experiments in data density and richness. The accuracy of CFD simulation has been confirmed by experimental studies [43–45]. In this paper, curved tunnel fires with vehicle blockage are explored, for which no experimental data are available in the existing literature. Therefore, experimental data related to straight tunnel fires with vehicle blockage are adopted to validate the numerical simulation method. Meng conducted a series of tests in a scaled model straight tunnel of 72 m × 1.5 m × 1.3 m ($L \times W \times H$) with vehicle blockage to investigate the temperature distribution of the tunnel ceiling for various heat release rates from the fire source, longitudinal air velocities, blocking ratios, and distances of the blockage from the fire source. A three-dimensional numerical model with a geometrical structure consistent with the laboratory tunnel model in the literature is built. The experimental results of the temperature distribution in the longitudinal centerline of the tunnel ceiling with a fire source power of 66.4 kW, a blocking ratio of 0.51, and a longitudinal air velocity of 0.48 m/s are selected to verify the numerical method, and the comparison between the simulation results and the experimental data of the literature is presented in Figure 7. The close agreement between the numerical simulations in this paper and the literature data, with maximum errors below 5%, indicates the suitability of the numerical method for simulating tunnel fires with vehicle blockage.

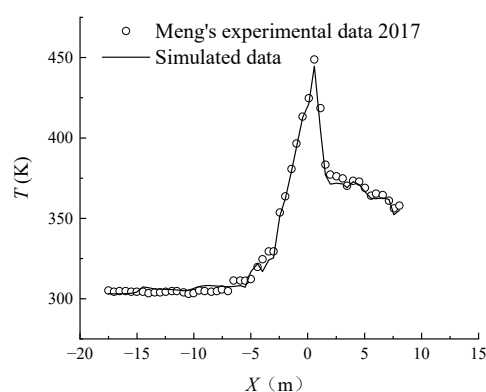


Figure 7. Comparison of CFD simulation and experimental results.

3. Results and Discussions

3.1. Flow Field Structure in Tunnel Fires

Figure 8 displays the flow field structure in a curved tunnel with a radius of 400 m, featuring a longitudinal air velocity of 2.0 m/s and a blocking ratio of 0.31. As the longitudinal airflow encounters the vehicle blockage, it accelerates due to the reduced cross-sectional area of the tunnel, in line with the continuity principle. This reduction also compresses the flow lines, leading to airflow separation at the blockage's start (point S) and the formation of recirculation I above the blockage. Further along, as the airflow moves past the vehicle obstruction, the tunnel's cross-sectional area suddenly increases and its geometry expands sharply, causing the airflow to separate again at the blockage's end (point E). Above this, a high-velocity free shear layer develops, while slower air downstream of the blockage generates recirculation II influenced by the shear layer. The free shear layer passes through the fire source and forms recirculation III at the tunnel ceiling. Vortices in recirculation I and II suck up the rising flame plume, exerting a pulling force upstream on the flame plume and deflecting it upstream. In recirculation III, the vortices exert a pulling force downstream on the flame plume, deflecting it downstream. Additionally, the inertia of free shear flow also causes the flame plume to deflect downstream.

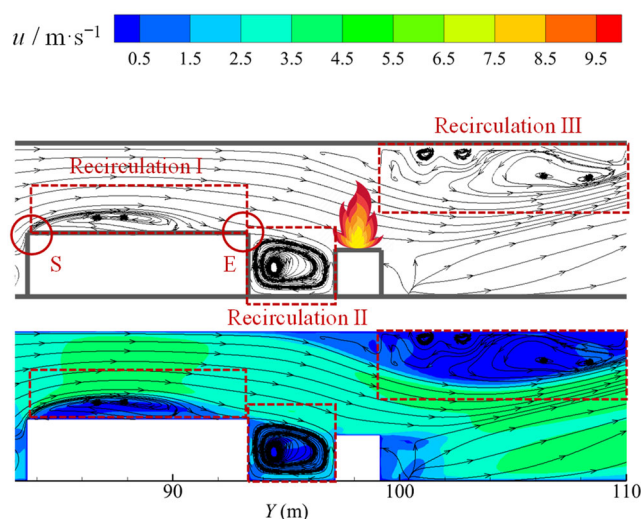


Figure 8. Flow structure of a curved tunnel with longitudinal air velocity $u = 2.0$ m/s, blocking ratio $\varphi = 0.31$, $R = 400$ m.

Figure 9 illustrates the flow field structure in a curved tunnel with a longitudinal air velocity of 2.0 m/s and various blocking ratios (0.31, 0.46, 0.55, 0.62). As the blocking ratio increases, the ventilation cross-section at the blockage decreases, and the physical compression causes the range of recirculation I at the top of the blockage to gradually decrease, while the range of recirculation II downstream of the blockage gradually expands. The speed of the free shear flow above the obstruction gradually increases, but most of the air in this region is adsorbed by the recirculation II and becomes a significant component of it, ultimately weakening the inertial force of the longitudinal wind on the fire plume in the downstream direction. Meanwhile, the position of the recirculation III gradually migrates upstream of the fire source and its range becomes smaller, thereby weakening the downstream pulling force on the fire plume.

Figure 10 displays the flow field structure in a curved tunnel with a blocking ratio of 0.46 and varying longitudinal air velocities (1 m/s, 2 m/s, 2.5 m/s, 3 m/s, 4 m/s). The diagram shows that as the longitudinal air velocity increases, the velocity in the free shear layer area also increases. Concurrently, the extent of recirculation I expands, recirculation II

behind the blockage slightly enlarges, and the flow becomes more turbulent. Additionally, the size of recirculation III significantly reduces until it eventually disappears.

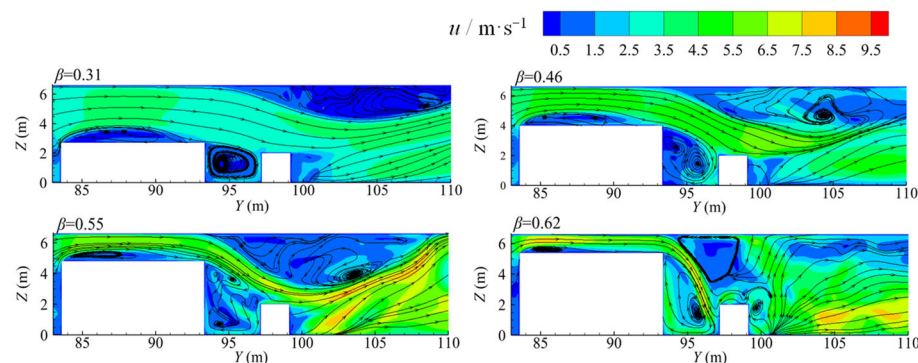


Figure 9. Flow field structure of curved tunnel for $u = 2.0$ m/s with different blocking ratios (0.31, 0.46, 0.55, 0.62).

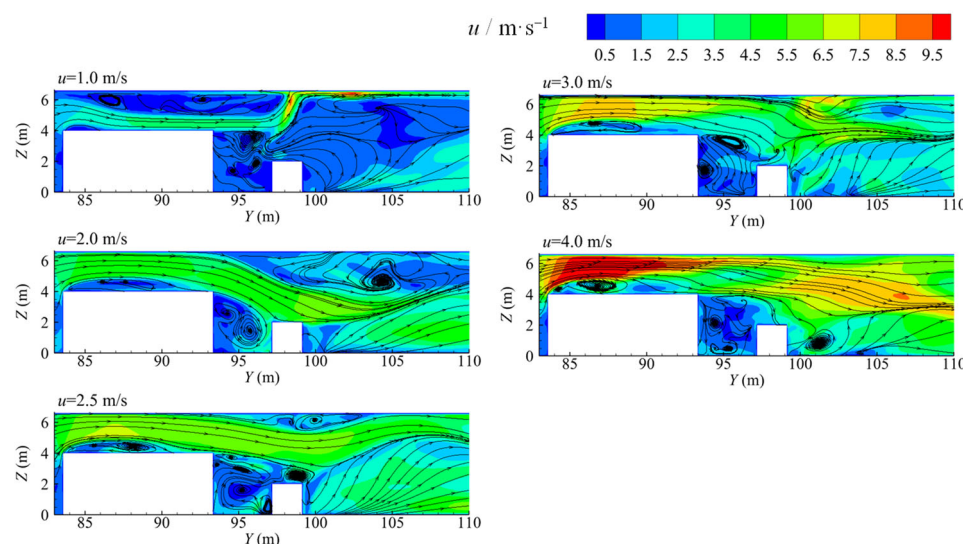


Figure 10. Flow field structure of a curved tunnel with different longitudinal air velocities at $\varphi = 0.46$.

In summary, the flow structure near vehicle obstructions and the fire source in curved tunnel fires (Figure 8) is complex. It includes a free shear layer, a recirculation zone above the vehicle blockage (I), a recirculation zone downstream of the blockage (II), and a recirculation zone at the top of the tunnel (III). The size of these three recirculation zones depends on the blocking ratio and longitudinal air velocity.

3.2. Characterization of Smoke Movement in Tunnel Fires

3.2.1. Impact of Curved Structures on Fire Plume Flow Behavior

The motion behavior of fire smoke is a key factor affecting the temperature distribution in the tunnel. This section primarily explores the influence of curved structures on the behavior of fire plume flow.

In a straight tunnel with $u = 1$ m/s, Figure 11 shows the temperature contour on the central axis plane of the tunnel (Figure 11a), the monitoring plane 0.01 m below the ceiling (Figure 11b), and the cross-section 2 m downstream of the fire source (Figure 11c) when the fire smoke reaches a quasi-steady state. The fire plume is visibly pushed downstream by its buoyancy and the wind force (Figure 11a). At the same time, under the influence of the longitudinal air flow, the smoke in the outer layer of the plume detaches from the main plume in the form of counter-rotating vortices. The resulting transverse drag

influence, upon reaching a certain intensity, leads to the lateral separation of the plume. The main body of the plume divides into two sub-streams, forming a bifurcated plume pattern (Figure 11c) [41]. Once the two sub-streams impact the tunnel ceiling, two impact points will be generated, forming two symmetrical high-temperature zones (Figure 11b).

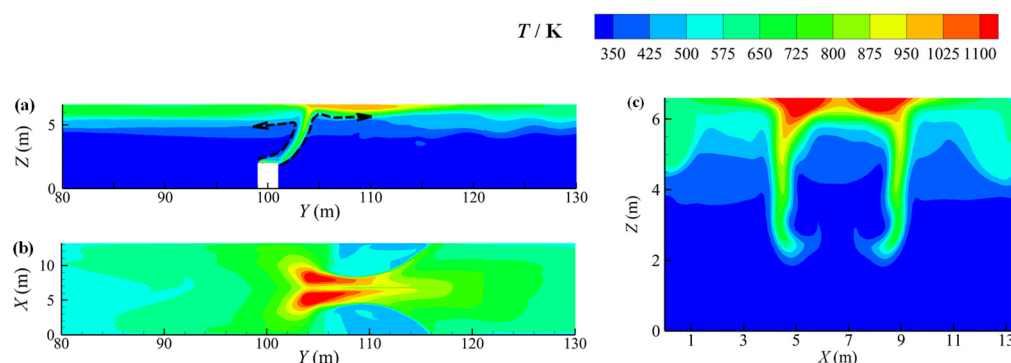


Figure 11. Temperature contours in a straight tunnel: (a) the central axis plane of the tunnel; (b) the monitoring plane 0.01 m below the ceiling; (c) the cross-section 2 m downstream of the fire source.

In a curved tunnel with a longitudinal air velocity of $u = 1$ m/s and $R = 400$ m, once the fire smoke reaches a quasi-steady state, Figures 12 and 13 show the temperature distribution along the tunnel's central axis, 2 m downstream from the fire source, and 0.01 m beneath the tunnel ceiling. Similar to a straight tunnel, the fire plume is deflected downstream by its buoyancy and wind forces (Figure 12), exhibiting bifurcation as it rises (Figure 13a–c).

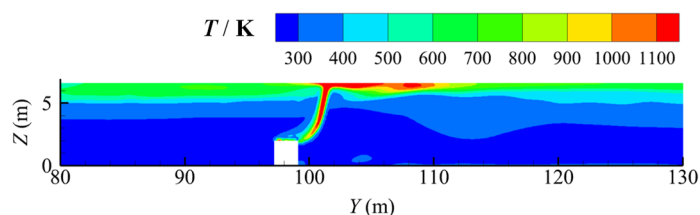


Figure 12. Temperature contour of the longitudinal central axis plane in a curved tunnel.

However, in contrast to straight tunnels, fire smoke in curved tunnels is not only affected by its own buoyancy and longitudinal wind but also by the centrifugal force resulting from the tunnel's curvature. This gives rise to dynamic deflection of the fire plume between the concave wall and the convex wall of the tunnel, modifying the location where it impacts the ceiling and generating diverse high-temperature zones. For instance, at 343 s after the fire, the two sub-streams are symmetrically distributed (Figure 13a), forming high-temperature zones on each side of the central axis on the tunnel ceiling (Figure 13d); at 393 s after the fire, the fire plume is deflected towards the convex wall (Figure 13b), creating a high-temperature zone nearby (Figure 13e); at 417 s after the fire, the fire plume shifts towards the concave wall (Figure 13c), forming a high-temperature zone there (Figure 13f). Once the fire smoke reached the quasi-steady state, temperature contours were recorded every second for two minutes, revealing that the plume deflected towards the concave wall 27% of the time, towards the convex wall 25% of the time, and remained at the median axis 49% of the time.

In summary, unlike the conventional fire scenarios in linear tunnels, where the maximum temperature in the vault is always located in the middle of the tunnel or symmetrically distributed along the centerline of the tunnel [41], the centrifugal force of the curved structure makes the location of the high-temperature zone in the vault constantly change, even in the quasi-steady state phase. This makes the maximum temperature rise in the vault of the curved tunnel more difficult to predict.

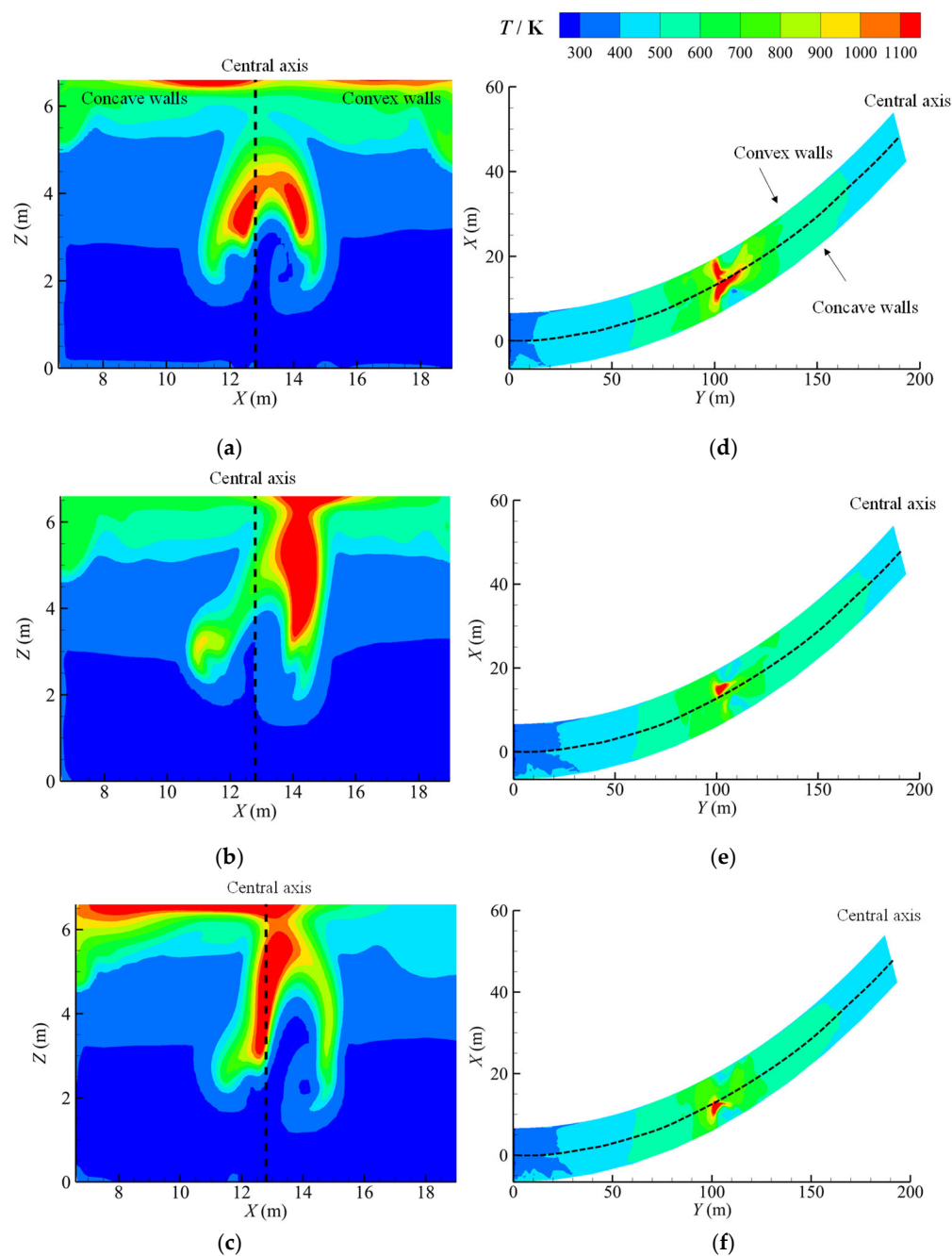


Figure 13. Temperature contour of the cross-section 2 m downstream of the fire source and the monitoring surface 0.01 m below the ceiling in a curved tunnel: (a) 2 m downstream from the fire source at 343 s; (b) 2 m downstream from the fire source at 393 s; (c) 2 m downstream from the fire source at 417 s; (d) 0.01 m beneath the tunnel ceiling at 343 s; (e) 0.01 m beneath the tunnel ceiling at 393 s; (f) 0.01 m beneath the tunnel ceiling at 417 s.

3.2.2. Effects of the Coupling Between Curved Structures and Blockages on Fire Plume Flow Behavior

This section focuses on the longitudinal and lateral movement characteristics of tunnel fire plumes affected by the interaction of blockages and curved structures. Figure 14 shows the temperature distribution cloud of the monitoring surface at 0.01 m below the tunnel vault surface in a curved tunnel with longitudinal wind speed $u = 1$ m/s and $R = 400$ m, built-in vehicle obstruction, and obstruction ratios φ of 0.31, 0.46, 0.55, and 0.62, respectively. It can be seen that when the fire smoke reaches the quasi-stable state, under the combined effect of the blockage effect and centrifugal force of the curved structure, the dynamic

deflection of the fire plume will also occur between the concave wall and the convex wall of the tunnel, thus changing the position of the fire plume impacting the tunnel vault, so that the position of the high-temperature zone on the tunnel vault surface constantly changes. Figure 15 shows the temperature distribution contour curve at 0.01 m below the tunnel vault, 2 m downstream of the fire source, corresponding to the blockage ratio of 0.46 for a curved tunnel with longitudinal wind speed $u = 1$ m/s and $R = 400$ m. It can be seen that the temperature zone on the surface of the tunnel vault constantly changes after a fire has occurred in the 3.5 m tunnel. It can be seen that the maximum temperature rise of the tunnel vault 2 m downstream of the fire source is shifted toward the concave wall at 383 s after the fire; the maximum temperature rise of the tunnel vault 2 m downstream of the fire source is almost located on the center axis of the tunnel vault at 402 s after the fire; and the maximum temperature rise of the tunnel vault 2 m downstream of the fire source is shifted toward the convex wall at 410 s after the fire.

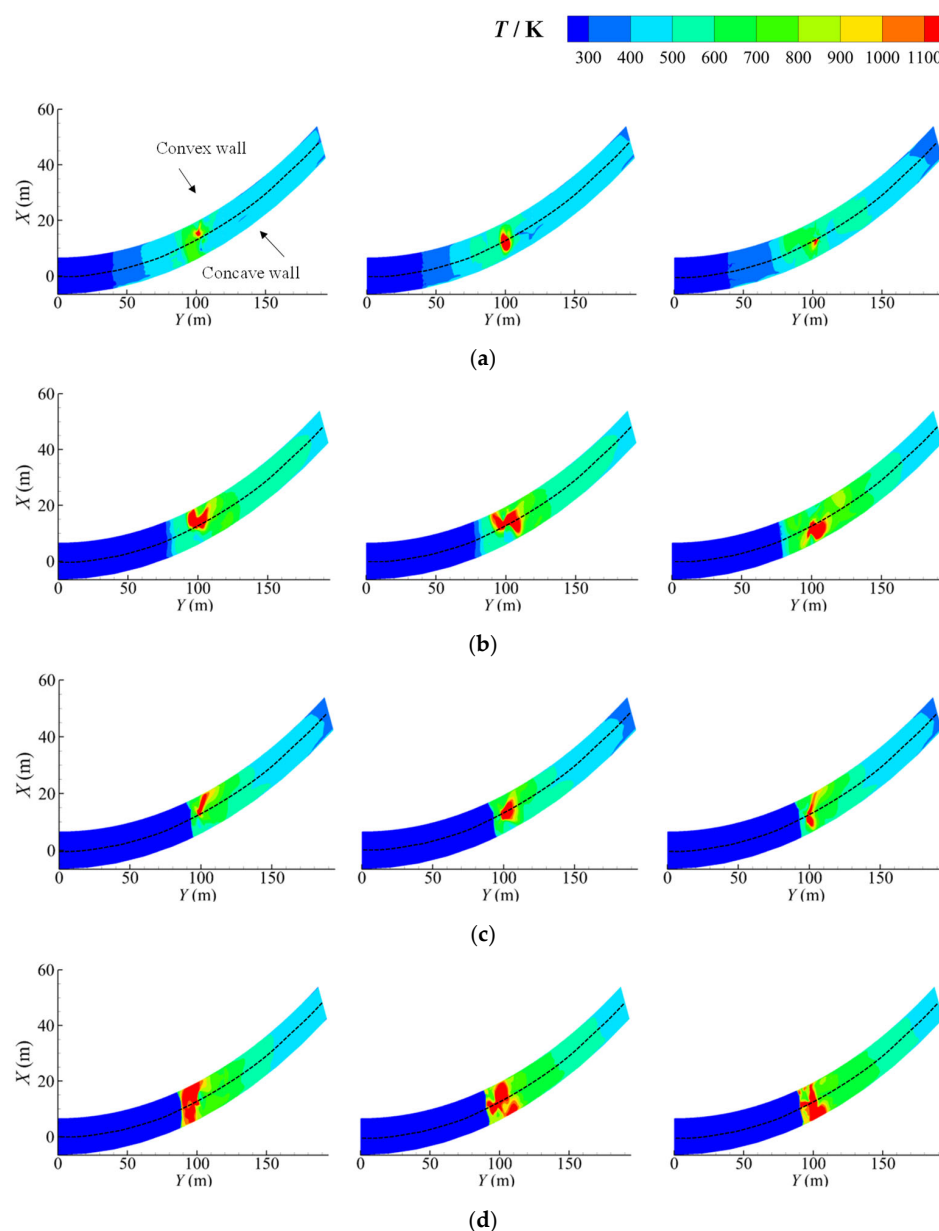


Figure 14. Temperature distribution on the arch surface of a curved tunnel with different blockage ratios for longitudinal wind speed $u = 1.0$ m/s: (a) $\varphi = 0.31$; (b) $\varphi = 0.46$; (c) $\varphi = 0.55$; (d) $\varphi = 0.62$.

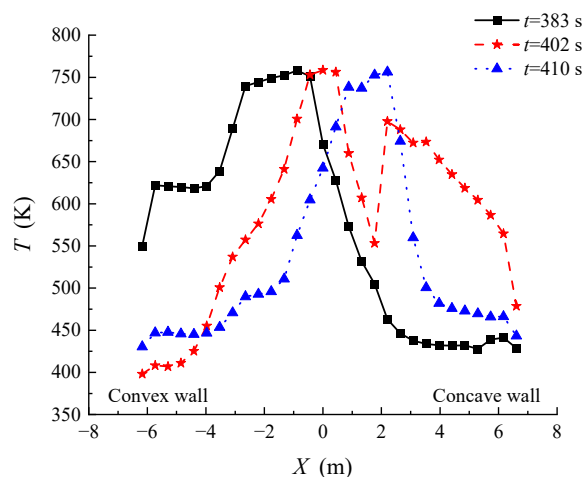


Figure 15. Temperature contours of the tunnel roof above the fire source under the obstruction ratio $\varphi = 0.46$ and longitudinal wind speed $u = 1.0$ m/s.

Given the instability of the lateral movement of fire plumes in curved tunnels, in this paper, the way to count the maximum temperature data of the vault of the curved tunnel is as follows: after the fire smoke reaches the quasi-stable state, collect the maximum temperature rise data of the whole vault surface of the tunnel for 2 min, and then take the time average value as the final maximum temperature rise of the tunnel vault. Figures 16 and 17 show the temperature maps of the longitudinal section of the curved tunnel and the maximum temperature rise of the tunnel vault under each condition when the blockage ratio is 0.31~0.62 and the longitudinal wind speed is 1 m/s~4 m/s. The maximum temperature rise of the tunnel vault under each condition is summarized in the following figures.

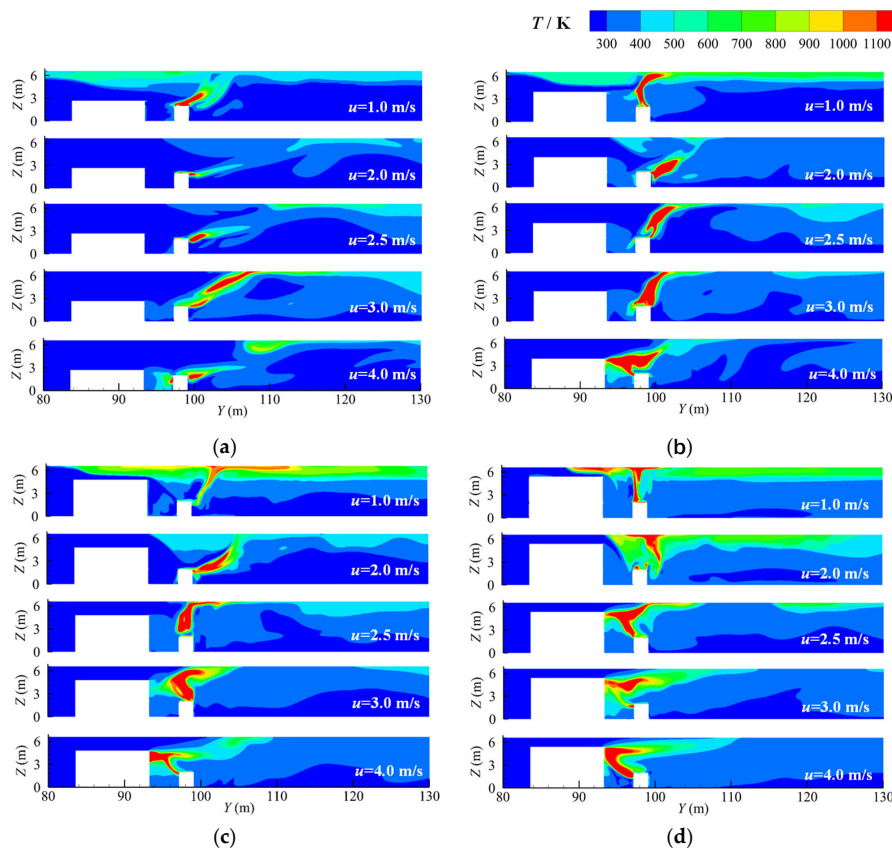


Figure 16. Fire plume behavior with different blocking ratios and ventilation air velocities: (a) $\varphi = 0.31$; (b) $\varphi = 0.46$; (c) $\varphi = 0.55$; (d) $\varphi = 0.62$.

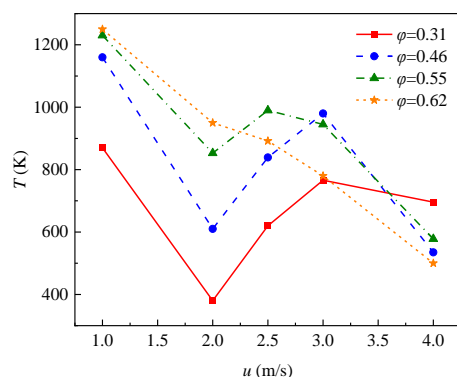


Figure 17. Maximum temperature rise in the tunnel ceiling.

From Figures 16a and 17, and the analysis in Section 3.1, it is evident that with a blocking ratio of $\phi = 0.31$ and ventilation air velocity $u \leq 2$ m/s, the pull force from the free shear layer and recirculation zone III on the fire plume is stronger than from recirculation zones I and II, causing the fire plume to tilt downstream. As ventilation air velocity increases, the stronger inertia from the free shear layer increases the tilt of the fire plume downstream, reducing the maximum temperature rise on the tunnel ceiling. When ventilation air velocity exceeds 2 m/s, the extent of recirculation I and II increases and becomes more turbulent, while recirculation III significantly decreases. This change weakens the downstream pull force on the fire plume, reducing its downstream tilt and thus increasing the maximum temperature rise on the ceiling. However, at 4 m/s, the fire plume's flow becomes highly turbulent. Influenced by recirculation I and II, parts of the plume shift upstream, but most of it remains tilted downstream. Since the tilt angle is larger than at 3 m/s, the maximum temperature rise on the ceiling slightly decreases.

From Figures 16b and 17, along with the analysis in Section 3.1, it is clear that with a blocking ratio of $\phi = 0.46$ and ventilation air velocity $u \leq 2$ m/s, the pull force from the free shear layer and recirculation zone III on the fire plume is stronger than from recirculation zones I and II, causing the fire plume to tilt downstream. As the ventilation air velocity increases, the stronger inertia from the free shear layer further tilts the fire plume downstream, reducing the maximum temperature rise on the tunnel ceiling. When the ventilation air velocity exceeds 2 m/s, the areas of recirculation I and II expand and become more turbulent, while recirculation III significantly contracts. This shift reduces the downstream pull force on the fire plume, decreasing its downstream tilt and causing a significant rebound in the maximum temperature rise on the ceiling, especially when the ventilation air velocity reaches 3 m/s, where the fire plume nearly touches the ceiling, reaching a peak temperature. At 4 m/s, recirculation zone III nearly vanishes, and the pull force from recirculation zones I and II becomes dominant, tilting the fire plume mostly upstream, which lowers the ceiling temperature.

From Figures 16c and 17 and the analysis in Section 3.1, it becomes apparent that with a blocking ratio of $\phi = 0.55$ and ventilation air velocity $u \leq 2$ m/s, the pull force from the free shear layer and recirculation zone III on the fire plume is stronger than from recirculation zones I and II, causing the fire plume to tilt downstream. As the ventilation air velocity increases, the stronger inertia from the free shear layer further tilts the fire plume downstream, reducing the maximum temperature rise on the tunnel ceiling. When the ventilation air velocity exceeds 2 m/s, the areas of recirculation I and II expand and become more turbulent, while recirculation III significantly contracts. This shift reduces the downstream pull on the fire plume, decreasing its downstream tilt. At air velocities of 2.5 m/s and 3 m/s, the fire plume nearly reaches the ceiling, causing a significant increase in the maximum temperature rise. At 4 m/s, recirculation zone III nearly vanishes, and the

pull force from recirculation zones I and II becomes dominant, tilting the fire plume mostly upstream, which lowers the ceiling temperature.

From Figures 16d and 17, along with the analysis in Section 3.1, it is clear that with a blocking ratio of $\varphi = 0.62$ and a ventilation air velocity of 1 m/s, the pulling forces from the free shear layer and recirculation zone III on the fire plume are similar to those from recirculation zones I and II, causing the fire plume to nearly reach the ceiling. As the ventilation air velocity increases, the pulling force from recirculation zones I and II strengthens, while the influence of recirculation zone III diminishes, leading to a weakened pull on the fire plume. This causes the fire plume to increasingly tilt upstream as the air velocity increases, resulting in a larger upstream tilt angle and a corresponding decrease in the tunnel ceiling’s temperature.

In summary, in a curved tunnel with a vehicle blockage upstream of the fire, the fire plume’s tilt direction shifts from downstream to upstream as the longitudinal air velocity increases. This results in a pattern where the plume first tilts downstream, then rises above the fire source to touch the ceiling, and finally tilts upstream. Consequently, the maximum temperature rise on the tunnel ceiling initially decreases, then increases, and finally decreases again. This pattern occurs because, in curved tunnels with vehicle blockages, the fire plume is influenced by opposing forces; recirculation zones I and II pull the plume upstream, while the free shear layer and recirculation zone III pull it downstream. The ultimate tilt direction of the plume depends on the relative strengths of these opposing forces.

Additionally, the higher the blocking ratio, the lower the critical air velocity needed for the fire plume to change its tilt from upstream to downstream. Specifically, the critical velocities for blocking ratios of 0.46, 0.55, and 0.62 are 3 m/s, 2.5 m/s, and 1 m/s, respectively. This occurs because a higher blocking ratio at a given air velocity enlarges the range and intensifies the turbulence in recirculation II, increasing its disruptive effect on the fire plume. Simultaneously, it reduces recirculation III, diminishing the downstream pulling force on the fire plume, making it easier for the plume to tilt upstream.

3.3. Maximum Temperature Rise of the Tunnel Arch

Meng studied a fire scenario in a straight tunnel with blocking vehicles (blocking ratio ranged from 0.24 to 0.72) and longitudinal wind (1 m/s to 4 m/s) and provided a prediction formula for the maximum ceiling temperature in this fire scenario [37]. Figure 18 contrasts the simulated maximum temperature rise of the ceiling with the projections from Meng’s [37] equation. The simulated values are typically higher than Meng’s predictions. This disparity occurs as Meng’s formula is founded on data from a straight tunnel and it modifies Li’s [17] formula. In curved tunnels, the fire plume osculates laterally between the concave and convex walls due to centrifugal forces, inducing smoke accumulation and reducing heat dissipation, which leads to higher ceiling temperatures [31].

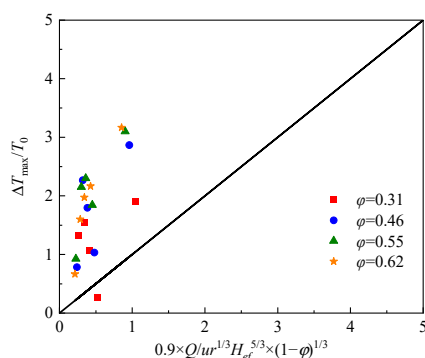


Figure 18. Comparison between the simulated data and Meng’s predicted data.

Based on the numerical simulation data in this paper and Li's formula [17], a predictive formula for the maximum temperature rise on the ceiling of a curved tunnel is obtained by introducing the non-dimensional velocity u^* (preferably u/\sqrt{gH}) and the blockage ratio φ , as shown in Equation (7). The comparison between the calculated and simulated results is depicted in Figure 19, with a fit R^2 of 0.96.

$$\frac{\Delta T_{max}}{T_0} = 17.65 \frac{Q}{ur^{1/3}H_{ef}^{5/3}} (1 - \varphi)^{1.053} \left(\varphi^{-0.2715} - 18.12u^* + 48.84u^{*2} - 36.81u^{*3} + 15.06\varphi u^* - 21.25\varphi u^{*2} \right) \quad (7)$$

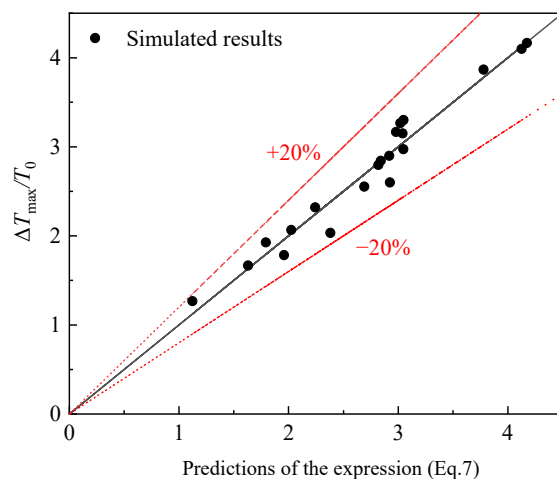


Figure 19. Numerical simulation and predictive model correlation.

4. Conclusions

This paper is the first to investigate the plume behavior and maximum ceiling temperature rise with various blockage ratios and ventilation conditions in curved tunnel fire scenarios, and it has established corresponding semi-empirical prediction models. This work emphasizes the intricate and unstable behavior of plumes in complex tunnel fire situations, thereby offering enhanced insights for the advancement of classical tunnel fire dynamic systems. The major findings are listed below:

1. After the fire smoke in the tunnel reaches a quasi-stable state, the high-temperature zone in the vault of a straight tunnel remains unchanged. However, for curved tunnels, in addition to its own buoyancy and longitudinal wind inertia forces, the fire smoke in curved tunnels is also affected by centrifugal forces induced by the curved structure. This results in a lateral dynamic deflection of the fire plume between the concave and convex walls of the tunnel, which changes the location of the fire plume impacting the tunnel vault and keeps the location of the high-temperature zone on the tunnel vault surface under dynamic change.
2. For curved tunnel fires with vehicle blockage, the flow structure in the near field of the blockage and fire source is very complex. It contains a free shear layer, recirculation I above the vehicle blockage, recirculation II downstream of the blockage, and recirculation III at the top of the tunnel. The extents of these recirculation zones depend on the blockage ratio and longitudinal air velocity. Higher air velocities lead to larger recirculation zones I and II but a smaller zone III, while a higher blockage ratio results in an expanded zone II and reduced zones I and III.
3. In the curved tunnel fire with vehicle blockages, the fire plume deflection direction changes from downstream to upstream of the fire source as the longitudinal air velocity increases, displaying a “downstream tilt—touch the ceiling above the fire source—upstream tilt” pattern. The maximum ceiling temperature rise fluctuates in

a decreasing-increasing-decreasing trend. A higher blockage ratio leads to a lower critical air velocity required for the transition of the plume deflection direction. This phenomenon results from the competing pulling forces acting on the fire plume within the tunnel: recirculation I and II pull the plume upstream, while the free shear layer and recirculation III pull it downstream. The ultimate plume deflection direction depends on the relative strengths of these opposing forces. A semi-empirical prediction model is developed to estimate the maximum temperature rise of a curved tunnel ceiling. This model accounts for both longitudinal wind effects and vehicle blockage ratios, showing strong agreement with numerical simulation results.

4. It should be noted that the degree of curvature of the curved tunnel, i.e., the curvature radius, will also have an impact on the behavior of tunnel fire plumes and the maximum ceiling temperature, and we will conduct a systematic and in-depth study on this in the follow-up. In addition, given the fact that the plume temperature is dominated by the entrainment process when rising, the theoretical prediction equation with more comprehensive physical significance will be established by solving the entrainment intensity of the major vortex quantitatively in our future work.

Author Contributions: Investigation, conceptualization, writing—original draft, writing—review and editing, funding acquisition, X.Z.; investigation, writing—original draft, formal analysis, J.L. and H.H.; conceptualization, writing—review and editing, X.C.; writing—review and editing, K.Z.; methodology, validation, M.Y.; investigation, formal analysis, Y.C.; conceptualization, writing—review and editing, funding acquisition, K.W. All authors have read and agreed to the published version of the manuscript.

Funding: This research was supported by the National Natural Science Foundation of China under Grant number 52408439, the National Natural Science Foundation of China under Grant number 52478422, and the Natural Science Basic Research Program of Shaanxi (Program No.2023-JC-YB-378).

Institutional Review Board Statement: Not applicable.

Informed Consent Statement: Not applicable.

Data Availability Statement: Data will be made available on request.

Conflicts of Interest: The authors declare that they have no conflict of interest, and that there are no conflicts of interest between them and Zhejiang University Urban and Rural Planning and Design Research Institute Co., Ltd.

References

1. Zhao, J.; Xu, Z.; Fang, L.; Zhang, Y.; Yu, C. Analyzing the reflash feature of large-area liquid fire in channel-like structures: A case study. *Case Stud. Therm. Eng.* **2022**, *38*, 102342. [[CrossRef](#)]
2. Zhang, X.; Guo, S.; Dang, X.; Hwang, A.; Li, F.; Yang, B.; Quan, C. Experimental investigation on the influence of portal-blocking speed on fire behaviors in tunnel structure. *Case Stud. Therm. Eng.* **2024**, *53*, 103811. [[CrossRef](#)]
3. Gao, Z.; Liu, M.; Zhao, P.; Yan, C. Influence of tunnel slope on the one-dimensional spread of smoke transportation and temperature distribution in tunnel fires. *Tunn. Undergr. Sp. Technol.* **2024**, *146*, 105650. [[CrossRef](#)]
4. Jiang, X.; Chen, X.; Xiao, N.; Liao, X.; Fan, C. Influence of the competitive effect of V-shaped slope tunnel on smoke characteristics. *Tunn. Undergr. Sp. Technol.* **2021**, *118*, 104193. [[CrossRef](#)]
5. Byrne, E.; Georgieva, K.; Carvel, R. Fires in ducts: A review of the early research which underpins modern tunnel fire safety engineering. *Tunn. Undergr. Sp. Tech.* **2018**, *81*, 306–314. [[CrossRef](#)]
6. Zhang, T.; Wang, G.; Hu, H.; Huang, Y.; Zhu, K.; Wu, K. Study on temperature decay characteristics of fire smoke backflow layer in tunnels with wide-shallow cross-section. *Tunn. Undergr. Sp. Tech.* **2021**, *112*, 103874. [[CrossRef](#)]
7. Chen, C.K.; Xiao, H.; Wang, N.N.; Shi, C.; Zhu, C.; Liu, X. Experimental investigation of pool fire behavior to different tunnel-end ventilation opening areas by sealing. *Tunn. Undergr. Sp. Tech.* **2017**, *63*, 106–117. [[CrossRef](#)]
8. Cong, W.; Nie, S.; Li, X.; He, K.; Peng, W. Experimental study and newly proposed correlations for maximum ceiling gas temperature rise in tunnel fires with natural ventilation. *Case Stud. Therm. Eng.* **2024**, *55*, 104164. [[CrossRef](#)]

9. Yao, Y.; Wang, R.; Xia, Z.; He, K.; Peng, W. Smoke movement and control in longitudinal ventilated tunnel fires with cross-passages. *Case Stud. Therm. Eng.* **2023**, *45*, 102945. [[CrossRef](#)]
10. Yao, Y.; He, K.; Peng, M.; Shi, L.; Cheng, X. The maximum gas temperature rises beneath the ceiling in a longitudinal ventilated tunnel fire. *Tunn. Undergr. Sp. Technol.* **2021**, *108*, 103672. [[CrossRef](#)]
11. Zhang, T.; Wang, G.; Li, J.; Wu, K.; Wang, L. Modelling the maximum ceiling temperature with bifurcated plume in tunnel fires. *Fire Saf. J.* **2024**, *150*, 104249. [[CrossRef](#)]
12. Wu, K.; Li, J.; Chen, X.; Duan, X.; Zhang, T.; Wang, L. Flame behavior and maximum ceiling temperature in traffic merging section tunnel fires: An experimental study and engineering modelling methodology. *Tunn. Undergr. Space Technol.* **2025**, *156*, 106230. [[CrossRef](#)]
13. Morton, B.R.; Taylor, G.I.; Turner, J.S. Turbulent gravitational convection from maintained and instantaneous sources. *Proc. R. Soc. Lond. Proc. Math. Phys. Eng. Sci.* **1956**, *234*, 1–23.
14. Zukoski, E.E.; Kubota, T.; Cetegen, B. Entrainment in fire plumes. *Fire Saf. J.* **1981**, *3*, 107–121. [[CrossRef](#)]
15. Alpert, R.L. Turbulent ceiling-jet induced by large-scale fires. *Combust. Sci. Technol.* **1975**, *11*, 197–213. [[CrossRef](#)]
16. Kurioka, H.; Oka, Y.; Satoh, H.; Sugawa, O. Fire properties in near field of square fire source with longitudinal ventilation in tunnels. *Fire Saf. J.* **2003**, *38*, 319–340. [[CrossRef](#)]
17. Li, Y.Z.; Lei, B.; Ingason, H. The maximum temperature of buoyancy-driven smoke flow beneath the ceiling in tunnel fires. *Fire Saf. J.* **2011**, *46*, 204–210. [[CrossRef](#)]
18. Ji, J.; Fu, Y.; Li, K.; Sun, J.; Fan, C.; Shi, W. Experimental study on behavior of sidewall fires at varying height in a corridor-like structure. *Proc. Combust. Inst.* **2015**, *35*, 2639–2646. [[CrossRef](#)]
19. Chen, L.; Tang, F.; Wang, Q.; Li, L. Experimental study on temperature distribution of ceiling jet in tunnel fires under natural ventilation. *Procedia Eng.* **2018**, *211*, 674–680. [[CrossRef](#)]
20. Li, L.; Cheng, X.; Cui, Y.; Dong, W.; Mei, Z. Effect of blockage ratio on the maximum temperature under the ceiling in tunnel fires. *J. Fire Sci.* **2013**, *31*, 245–257. [[CrossRef](#)]
21. Zhong, W.; Liu, L.; Han, N.; Gao, Z.; Zhao, J. Investigation on the maximum ceiling temperature of the weak plume impingement flow in tunnel fires under longitudinal ventilation. *Tunn. Undergr. Sp. Technol.* **2023**, *131*, 104821. [[CrossRef](#)]
22. Tian, X.L.; Zhong, M.H.; Liu, C.; Li, Q. A full-scale experimental study of tunnel fire under different blockage conditions. *Coal Sci. Technol.* **2021**, *49*, 93–101.
23. Shafee, S.; Yozgatligil, A. An analysis of tunnel fire characteristics under the effects of vehicular blockage and tunnel inclination. *Tunn. Undergr. Sp. Technol.* **2018**, *79*, 274–285. [[CrossRef](#)]
24. Han, J.; Wang, F.; Wen, J.; Liu, F.; Ma, W.; Wang, Z.; Ma, Z. Investigation on the characteristics of fire burning and smoke spreading in longitudinal-ventilated tunnels with blockages. *Tunn. Undergr. Sp. Technol.* **2023**, *131*, 104790. [[CrossRef](#)]
25. Hu, L.H.; Tang, W.; Chen, L.F.; Yi, L. A non-dimensional global correlation of maximum gas temperature beneath ceiling with different blockage–fire distance in a longitudinal ventilated tunnel. *Appl. Therm. Eng.* **2013**, *56*, 77–82. [[CrossRef](#)]
26. Tang, F.; Cao, Z.L.; Chen, Q.; Meng, N.; Wang, Q.; Fan, C. Effect of blockage-heat source distance on maximum temperature of buoyancy-induced smoke flow beneath ceiling in a longitudinal ventilated tunnel. *Int. J. Heat. Mass. Tran.* **2017**, *109*, 683–688. [[CrossRef](#)]
27. Gannouni, S.; Maad, R.B. Numerical study of the effect of blockage on critical velocity and backlayering length in longitudinally ventilated tunnel fires. *Tunn. Undergr. Sp. Technol.* **2015**, *48*, 147–155. [[CrossRef](#)]
28. Zhang, S.; Cheng, X.; Yao, Y.; Zhu, K.; Li, K.; Lu, S.; Zhang, R.; Zhang, H. An experimental investigation on blockage effect of metro train on the smoke back-layering in subway tunnel fires. *Appl. Therm. Eng.* **2016**, *99*, 214–223. [[CrossRef](#)]
29. Meng, N.; Yang, W.; Xin, L.; Li, X.; Liu, B.; Jin, X. Experimental study on backlayering length of thermal smoke flow in a longitudinally ventilated tunnel with blockage at upstream of fire source. *Tunn. Undergr. Sp. Technol.* **2018**, *82*, 315–324. [[CrossRef](#)]
30. Tang, W.; Hu, L.H.; Chen, L.F. Effect of blockage-fire distance on buoyancy driven back-layering length and critical velocity in a tunnel: An experimental investigation and global correlations. *Appl. Therm. Eng.* **2013**, *60*, 7–14. [[CrossRef](#)]
31. Guo, J.; Cai, G.; Liu, Y.; Wen, H.; Jin, Y. Temperature distribution and characteristics induced by fire smoke in L-shaped utility tunnels with small curvature radii. *Case Stud. Therm. Eng.* **2021**, *28*, 101470. [[CrossRef](#)]
32. Guo, J.; Gao, W.; Cai, G.; Liu, Y.; Wen, H. Numerical study on fire-induced smoke temperature characteristics in small curvature radius UTLT-like tunnels under emergency state. *Tunn. Undergr. Sp. Technol.* **2022**, *127*, 104599. [[CrossRef](#)]
33. Tao, W.Q. *Numerical Heat Transfer*, 2nd ed.; Xi'an Jiaotong University Press: Xi'an, China, 2001.
34. Shih, T.H.; Zhu, J.; Lumley, J.L. A new Reynolds stress algebraic equation model. *Comput. Methods. Appl. Mech. Eng.* **1995**, *125*, 287–302. [[CrossRef](#)]
35. Meseguer, J.; Pérez-Grande, I.; Sanz-Andrés, A. *Spacecraft Thermal Control*; Elsevier: Amsterdam, The Netherlands, 2012; pp. 73–86.
36. Huang, Y.B.; Lu, S.R.; Yang, K. Research on the influence of fire source power and tunnel obstruction ratio on the change rule of critical wind speed. *China Saf. Prod. Sci. Technol.* **2015**, *11*, 10–15.

37. Meng, N.; Liu, B.; Li, X.; Jin, X.; Huang, Y.; Wang, Q. Effect of blockage-induced near wake flow on fire properties in a longitudinally ventilated tunnel. *Int. J. Therm. Sci.* **2018**, *134*, 1–12. [[CrossRef](#)]
38. Stroup, D.; Lindeman, A. *Verification and Validation of Selected Fire Models for Nuclear Power Plant Applications*; U.S. Nuclear Regulatory Commission (NRC): Washington, DC, USA, 2013.
39. He, L.; Xu, Z.; Chen, H.; Liu, Q.; Wang, Y.; Zhou, Y. Analysis of entrainment phenomenon near mechanical exhaust vent and a prediction model for smoke temperature in tunnel fire. *Tunn. Undergr. Sp. Technol.* **2018**, *80*, 143–150. [[CrossRef](#)]
40. Su, Z.; Li, Y.; Zhong, H.; Li, J.; Guo, Z.; Yang, X.; Yang, S. Advancements in smoke control strategies for metro tunnel cross-passage: A theoretical and numerical study on critical velocity and driving force. *Tunn. Undergr. Sp. Technol.* **2024**, *147*, 105734. [[CrossRef](#)]
41. Wu, K.; Wang, G.; Li, J.; Huang, Y.; Yan, X.; Zhang, T. Numerical study on plume bifurcation in longitudinally ventilated tunnel fires. *Tunn. Undergr. Space Technol.* **2023**, *132*, 104926. [[CrossRef](#)]
42. Wu, K.; Chen, X.; Li, J.; Zhang, L.; Zhu, K.; Hong, Y.; Zhang, T. Flame behavior and fire-induced flow field characteristic in building corridor fire with longitudinal partition. *J. Build. Eng.* **2023**, *76*, 107358. [[CrossRef](#)]
43. Weng, M.C.; Lu, X.L.; Liu, F.; Shi, X.P.; Yu, L. Prediction of backlayering length and critical velocity in metro tunnel fires. *Tunn. Undergr. Sp. Technol.* **2015**, *47*, 64–72. [[CrossRef](#)]
44. Hu, L.H.; Huo, R.; Chow, W.K. Studies on buoyancy-driven back-layering flow in tunnel fires. *Exp. Therm. Fluid. Sci.* **2008**, *32*, 1468–1483. [[CrossRef](#)]
45. Colella, F.; Rein, G.; Borchiellini, R.; Torero, J. A novel multiscale methodology for simulating tunnel ventilation flows during fires. *Fire Technol.* **2011**, *47*, 221–253. [[CrossRef](#)]

Disclaimer/Publisher’s Note: The statements, opinions and data contained in all publications are solely those of the individual author(s) and contributor(s) and not of MDPI and/or the editor(s). MDPI and/or the editor(s) disclaim responsibility for any injury to people or property resulting from any ideas, methods, instructions or products referred to in the content.